The complex life of MTOR

Rehbein, Ulrike

DOI:
10.33612/diss.147590696

Chapter 3

Breaking the interface: efficient extraction of magnetic beads from nanoliter-droplets for automated sequential immunoassays

Lukas Metzler[$,1], **Ulrike Rehbein**[$,2,3], Jan-Niklas Schönberg[1], Thomas Brandstetter*[,1], Kathrin Thedieck*[,#,2,3,4], Jürgen Rühe*[,#,1]

[1]Chemistry & Physics of Interfaces, Department of Microsystems Engineering - IMTEK, University of Freiburg, 79110 Freiburg, Germany

[2]Department of Neuroscience, School of Medicine and Health Sciences, Carl von Ossietzky University Oldenburg, 26129 Oldenburg, Germany

[3]Laboratory of Pediatrics, Section Systems Medicine of Metabolism and Signaling, University of Groningen, University Medical Center, 9700 AB Groningen, The Netherlands

[4]Institute of Biochemistry and Center for Molecular Biosciences Innsbruck, University of Innsbruck, 6020 Innsbruck, Austria

$, # These authors contributed equally

*Correspondence: ruehe@imtek.uni-freiburg.de, kathrin.thedieck@uibk.ac.at, k.thedieck@umcg.nl, kathrin.thedieck@uni-oldenburg.de

Published in “Analytical Chemistry”. PMID: 32501674

Abstract

Droplet-based microfluidic systems offer a high potential for miniaturization and automation. Therefore, they are becoming an increasingly important tool in analytical chemistry, biosciences, and medicine. Heterogeneous assays commonly utilize magnetic beads as a solid phase. However, the sensitivity of state of the art microfluidic systems is limited by the high bead concentrations required for efficient extraction across the water−oil interface. Furthermore, current systems suffer from a lack of technical solutions for sequential measurements of multiple samples, limiting their throughput and capacity for automation. Taking advantage of the different wetting properties of hydrophilic and hydrophobic areas in the channels, we improve the extraction efficiency of magnetic beads from aqueous nanoliter-sized droplets by 2 orders of magnitude to the low µg/mL range. Furthermore, the introduction of a switchable magnetic trap enables repetitive capture and release of magnetic particles for sequential analysis of multiple samples, enhancing the throughput. In comparison to conventional ELISA-based sandwich immunoassays on microtiter plates, our microfluidic setup offers a 25−50-fold reduction of sample and reagent consumption with up to 50 technical replicates per sample. The enhanced sensitivity and throughput of this system open avenues for the development of automated detection of biomolecules at the nanoliter scale.

Increasingly, droplet-based microfluidics is being recognized as a powerful tool for the analysis of biological samples. This technology offers multiple options to implement high throughput setups with a high degree of automation for analyses at the microscale. Hundreds to thousands of uniform aqueous droplets are employed to serve as individual micro-reactors for (bio)chemical assays.[1,2] The droplets are created at T-junctions, or more complex geometries, at which an aqueous solution joins an immiscible oil. Due to surface instabilities, the aqueous solution is sheared off into individual droplets carried downstream by the water-immiscible continuous phase.[3] The volume of the droplets is typically in the femto to nanoliter range, enabling assays with minimal sample consumption.[1,4] Multiple operations to manipulate the droplets, including merging, mixing, splitting, and sorting, have been established, and are frequently used for the implementation of state of the art immunoassays in microfluidics.[4–6] Thus, assay components can be added to individual droplets, and droplets carrying features of interest can be selected for analysis. If the droplets' dimensions are confined by the channel dimensions, they are often referred to as plugs.[7]

The implementation of biochemical assays in one homogeneous, liquid phase without intermittent washing steps has been well established for droplet microfluidics.[4,8] In contrast, heterogeneous assays allow the separation of the assay products from the unbound components which usually increases the sensitivity and specifity of an assay. On microtiter plates, repeated washing steps can be easily implemented by exchanging the liquid phase while performing immunoblots, enzyme-linked immunosorbent assays (ELISA), or fluorescence-based sandwich immunoassays. Therefore, they remain commonly used analysis methods, both in research and clinical analytics. However, in droplet-based approaches the separation of the assay product from the unbound components remains challenging. Overcoming this hurdle would be of great benefit for the field of analytical chemistry, especially when sample volumes and reagents are limited and high throughput is required.

In two-phase flow setups, functionalized magnetic beads are frequently used as a solid phase for heterogeneous affinity assays. They promise easy purification and isolation of the assay product from the aqueous reaction environment for downstream analysis.[9] However, magnetic bead extraction from aqueous droplets is limited by the high surface tension of the water−oil interface. As the efficiency of magnetic bead extraction is a key determinant of sensitivity in microfluidic systems, optimizing the bead extraction represents a potent means to enhance their performance.

One way to overcome this challenge is to avoid extraction altogether. This can be achieved by merging the aqueous droplets with the continuous aqueous phase, thus avoiding the need for particles to pass through the water−oil interface.[10] This strategy enables the analysis of low amounts of beads at the expense of losing the droplets in the continuous phase. This approach, however, excludes the option to analyze the droplet phase after the extraction or to reuptake the magnetic beads into another

droplet. To maintain the droplets' integrity, several studies have proposed droplet splitting to enrich the assay product. Therefore, droplets are divided at a T-junction, while steering the beads by magnetic force into one of the daughter droplets.[11–13] Even though this approach does reduce background signals from molecules dissolved in the aqueous phase, this concept by definition suffers from substantial residual contamination from the initial liquid phase.[12,13]

In spite of its shortcomings, magnetic bead extraction from the droplets still appears more promising than the aforementioned alternatives, as the major fraction of the liquid in the droplet is removed, and only residual amounts of the initial aqueous phase remain trapped between the closely packed magnetic beads.[14] Conceptually, this approach requires the extraction of the beads with the bound analyte by piercing the water−oil interface. In 2012, Ali-Cherif et al.[14] demonstrated an effective extraction of almost pure magnetic beads from nanoliter droplets. Magnetic coils with sharp tips served to focus the magnetic field and thereby enhance the magnetic force acting on the magnetic bead clusters.[14,15] For this kind of magnetic trap, a magnetic bead concentration of at least 1−10 mg/mL is required[14,16–18] to obtain the minimal cluster size that overcomes the interfacial barrier. While the magnetic force (F_M) and the mass (m) of an object scale with the size (d) in a cubic relation ($FM \sim m \sim d^3$), the surface tension (γ) scales with d in a linear manner ($\gamma \sim d^1$).[19] At low concentrations, only small bead clusters are formed, and thus, the surface tension exceeds the magnetic force. This prevents successful extraction of small bead quantities. Increasing the bead concentration, however, is not advantageous as the number of detectable molecules per bead decreases, whereas the increased number of beads results in a higher background signal and variance due to higher autofluorescence and/or light scattering. Both factors usually lead to an increase in the lower limit of detection (LoD).

To aid the transit through the water−oil interface, we previously suggested to add nonfunctionalized magnetic beads prior to the extraction of functionalized beads.[20] This strategy allows for the concentration of analyte molecules onto a small number of particles but still suffers from the need of a relatively large amount of beads at the point of detection - creating a substantial background signal. Furthermore, the additional step required prior to magnetic bead extraction hampers automation. Another concept to aid the breakup of the water−oil interface is the wetting of a hydrophilic channel by the aqueous phase.[21] This removes the interface between the droplet and the channel and thus reduces the force necessary to drag the magnetic particles to the channel wall. Schönberg et al.[22] demonstrated the potential to extract magnetic beads down to concentrations of 1 µg/mL while preserving the droplets' integrity. However, the compatibility of this concept with microfluidic immunoassays remains to be tested.

In this study, we describe a microfluidic setup that allows for the extraction of magnetic beads at low concentrations. We develop and validate the application for heterogeneous sandwich immunoassays at the nanoliter scale. To capture and

release magnetic beads, we introduce a magnetic trap that allows us to switch the local magnetic field on and off. We determine the influence of the assay parameters on the analytical performance, in particular, on the limit of detection (LoD).

CONCEPT AND OPERATING PRINCIPLE

Microfluidic Immunoassay. We base our microfluidic platform on the setup developed by Rendl et al.,[20] in which heterogeneous assays are performed in plugs serving as miniaturized reaction compartments. The system consists of perfluorinated tubings filled with perfluorocarbon carrier oil (FC-43 or FC-3283) and reagents in aqueous solution. The tubings are connected through T-junctions at which the aqueous solution flowing in becomes sheared off into the water-immiscible carrier oil, thereby forming nanoliter droplets. While the setup of Rendl et al.[20] consisted of one T-junction through which different reagents were added by repeated forward and backward flows, we combine here two T-junctions (**Figure 1**). This allows us to reduce the droplet movements to a minimum. First, we add an aqueous dispersion of magnetic beads coated with capture antibodies to the carrier oil, thereby generating plugs in reverse direction to flow 1 (**Figure 1**, yellow). After lining up of the plugs this way, the analyte containing sample(s) and detection antibodies are added to the plugs at the two T-junctions (**Figure 1**, flow 2 [blue] and 3 [red]). The flow speed is kept constant after the last merging step so that the incubation time is equal for each droplet immunoassay.

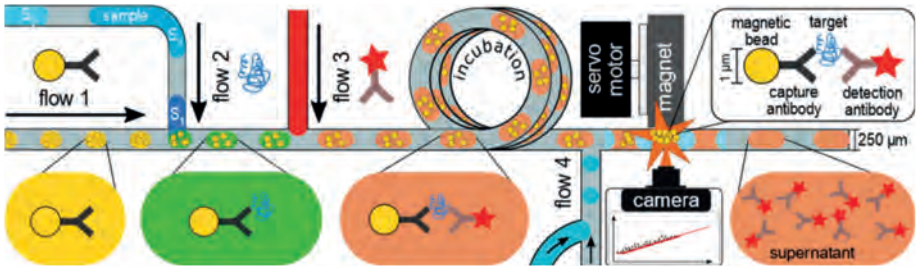

Figure 1. Illustration of the fluorescence-based sandwich immunoassays on magnetic beads in nanoliter droplets. The sample(s) (flow 2, shades of blue) and the detection antibody (flow 3, red) are added successively to a droplet train containing magnetic beads (flow 1, yellow). During incubation, the droplets move through the fluidic channel. A final wash step takes place at the magnetic trap, where the magnetic beads are separated from the supernatant. The accumulation of the fluorescence signal is recorded with an inverted microscope. Flow 4 aids to release of captured beads.

To setup and optimize this microfluidic system, a simplified assay with streptavidin and Atto-647N-Biotin (Atto-Biotin) was used. The streptavidin−biotin binding is the strongest known noncovalent interaction between biological molecules (K_D = 10^{-13} M).[23] This strong affinity allowed for optimization of the performance of the microfluidic system. Thus, plugs with streptavidin-coated beads (flow 1) were merged with Atto-

Biotin containing samples at the first T-junction (flow 2) and PBST (phosphate-buffered saline with 0.1% (v/v) Tween 20) at the second T-junction (flow 3). The latter was used for addition of detection antibody for sandwich immunoassays (see below, proof of concept).

The magnetic trap is a key feature of this microfluidic platform. For detection, the magnetic beads, carrying the assay product, must be extracted from the plugs, while the supernatant with unbound analyte and antibodies moves downstream. To this, two neodymium magnets were placed at either side of the tubing to capture the beads at the point of detection (marked by a orange star in **Figures 1** and **2a**). The two magnets are arranged such that they generate a magnetic field B, focused at the magnet edges (B_{max} = 1 T, **Figure 2b** [pink area] and **2c** [max. values on y-axis]). This two-magnet setup maximizes the gradient of the magnetic field and led to a well-defined area of extraction at the first peak of the magnetic field (**Figure 2c**) The position of the magnets is controlled by servomotors (**Figure 2a**) actuated by a programmable Arduino microcontroller. This allows for the synchronization of the magnetic trap to the flow pattern and can automatically open the magnetic trap after each measurement. Thus, the trapped beads can be released from the point of extraction, and subsequent droplets clear the tubing. An additional wash flow (**Figure 1**, flow 4) can further aid the release of the beads.

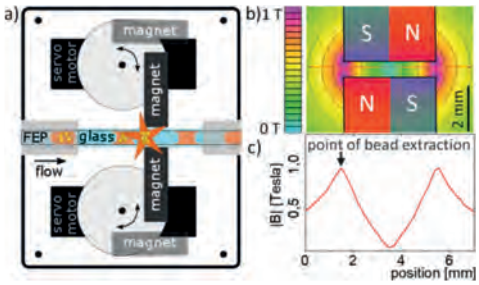

Figure 2. Magnetic trap. (a) Illustration of the magnetic trap for extraction of beads (yellow) from aqueous droplets (brown). Beads are kept stationary at the point of extraction/detection (orange star) by two servomotor-controlled magnets. FEP, fluorinated ethylene propylene tubing. (b) Simulation of the magnetic field lines for the two magnets in the magnetic trap. N, magnetic north. S, magnetic south. T, Tesla. (c) Simulated intensity of the magnetic field along the fluidic channel [red line in (b)]. The bead extraction takes place at the first maximum of the magnetic field. Arrow, point of bead extraction.

It is assumed that all the plugs carry the same average fluorophore load (i.e., fluorescent assay product). Therefore, as these fluorophores accumulate in the magnetic trap, a linear increase of the detection signal is expected. Thus, a linear regression can be used to evaluate the mean contribution of the droplets to the signal. In other words, the slope of the signal increase correlates to the amount of fluorescent assay product at the surface of the beads.

MATERIALS AND METHODS

Functionalization of Beads with Capture antibodies. The streptavidin-coated superparamagnetic beads (Dynabeads MyOne Streptavidin T1, #65601, Invitrogen, US) were functionalized with the biotinylated capture antibodies as recommended by the supplier (IL-6: antibody raised in goat against human IL-6, residues M1−M212, #BAF206, R&D, US; mTOR: Clone 3G6,[1] antibody raised in rat against human mTOR, residues T221−I260). The magnetic beads were washed twice with PBST and diluted to a concentration of 0.1 mg/mL. Capture antibodies were added in amounts exceeding the binding capacity of the beads and incubated for at least 30 min at room temperature with gentle agitation. Unbound antibodies were removed by three washes with PBST. Beads were reconstituted in PBST to the final concentration.

Microfluidic Procedure. The procedure consists of the following steps: (i) droplet generation in reverse direction to flow 1 (see **Figure 1**), (ii) addition of further reagents to the droplets at the T-junctions: merging with droplets containing sample and fluorophore-labeled detection antibodies or PBST (in the case of Atto-Biotin experiments), (iii) incubation at a constant flow rate; incubation times: Atto-Biotin experiments, t = 13.5 min; sandwich immunoassays, t = 27 min, and (iv) magnetic bead extraction and detection of the fluorescent signal at the magnetic trap. The magnetic beads of each sequence were sequentially accumulated in the magnetic trap. Opening and closing of the magnetic trap were synchronized with the fluidic workflow. Further details are given in the Results and Discussion section and in the Supporting Information, **Figure S-1**.

The platform consists of fluorinated ethylene propylene polymer (FEP) tubing (inner diameter 0.25 mm, outer diameter 1.60 mm, #2001001, PRO LIQUID GmbH, Germany) connected by CTFE T-junctions and union fittings (microvolume connector, 1/16 in.; 0.25 mm bore, VICI AG International, MT1CKF & MU1CKF, MACHEREY-NAGEL GmbH, Germany). Precise and programmable flow was enabled by neMESYS 290 N syringe pumps (#A3921000132, Cetoni GmbH, Germany).

Bead Extraction under Different Wetting Conditions. To compare the bead extraction in hydrophobic FEP tubes and hydrophilic glass capillaries, magnetic beads (c = 1 mg/mL) were stained with Atto-Biotin (red, #93606, Sigma-Aldrich, Germany) prior to droplet generation. To visualize the droplets, a Cy3-labeled oligonucleotide (green, Cy3-Oli3 (KK), 44 mer, #1916046, TIB Molbiol, Germany) was added to the aqueous solution; images were recorded using G-2A and Cy5-filters (four frames/s, flow rate = 1.5 µL/min).

Image and Data Analysis. The fluorescence intensities were analyzed with ImageJ (version 1.52d). Fluorescent signals were measured as the average pixel intensity for a rectangular area (region of interest, ROI). The signal slopes were fitted to the "lower enveloping curve", using the OriginPro 2019 (version 9.6.0.172) software. After plotting against the concentrations, the data was fitted by 4-Parameter logistic curves[24,25] using OriginPro 2019. Negative controls (c(target) = 0) were added as the lowest value in the dilution series.

Determination of the Lower Limit of Detection (LoD). The LoD was determined as detailed in the next section. The background signal was obtained by the sigmoidal fit. The indicated concentrations were derived from the intersection with the regression curve.

Hydrophobization of the Glass Capillaries. To obtain partially hydrophobic glass capillaries (2 µL minicaps, end to end, #L919.2, Hirschmann Laborgeräte GmbH & Co. KG, Germany), the capillaries were washed three times each with water, isopropanol/water (70:30, v/v), and isopropanol, and dried in a vacuum oven (60 °C) overnight. Next, the capillaries were placed upright into 200 µL PCR-tubes (781305, Brand GmbH, Germany), filled with 65 µL of a trichloro- (1H,1H,2H,2H-perfluorooctyl)silane solution (1 vol %, #448931, Sigma-Aldrich, Germany) in FC-3283. Thereby, approximately 19 mm of each capillary was filled. After 10 min at room temperature, the capillaries were washed with water and FC-3283 and dried with nitrogen. Thus, the length of the hydrophilic (untreated) part was limited to 13.2 ± 1.0 mm. As a result, the capillaries were only hydrophilic at the point of extraction.

Characterization of The Light Sources. The light source emission spectra were analyzed with a blue wave spectrometer (UVN-25, 600 g/mm, #16101419, StellarNet, Inc., USA) in combination with the Cy5 ET filter set. The fiber optics of the spectrometer were focused using the 4× objective.

RESULTS AND DISCUSSION

Bead extraction. The extraction of magnetic beads from a microfluidic water droplet is mainly limited by the surface tension of its interface to the surrounding carrier fluid. [14–18] To study the influence of the wetting properties of the microfluidic channels, the magnetic trap was initially operated with an unmodified hydrophobic channel (FEP tubing). We monitored the signal intensity in the region of interest (ROI). In this setup, the beads (c = 1 mg/mL) failed to penetrate the water− oil interface and remained in the droplets after passing the predicted point of extraction at the location of B_{max} (**Figure 3a** and **b**). Therefore, the fluorescent signal reflects only the droplets passing by (**Figure 3c**). Thus, we conclude that this setup does not

allow extracting beads at a concentration of 1 mg/mL or lower. This is in agreement with earlier studies.[10,14]

Schönberg et al.[22] have demonstrated that hydrophilic patches on the channel surface allow efficient extraction of low bead concentrations (≥1 µg/mL). In order to realize this strategy, we replaced part of the tubing by a hydrophilic glass capillary in the area of extraction. This change in the surface wetting led to an inverted shape of the aqueous droplets (**Figure 3d** and **e**) Thus, the beads no longer need to penetrate the droplet interface before they reach the channel wall and become captured. With the hydrophilic glass capillary, we observed an accumulation of the magnetic beads and consequently a linear stepwise of the fluorescence signal increase after every droplet passing the ROI (**Figure 3f**, and animation in Supporting Information). Clearly, the wetting of the channel facilitates the bead extraction.

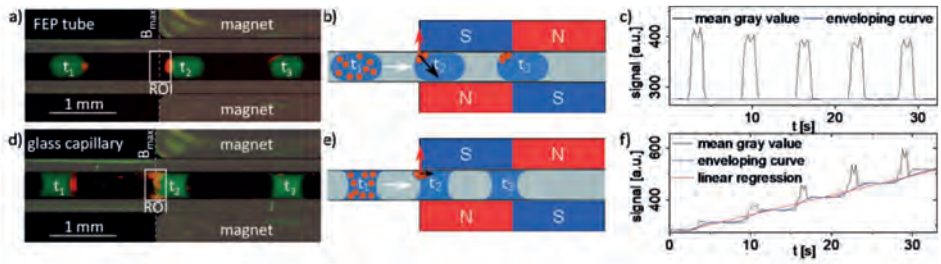

Figure 3. Magnetic bead extraction. (a,d) Attempts of magnetic bead extraction from nanoliter droplets in hydrophobic FEP tubes (a) and hydrophilic glass capillary (d) in the magnetic trap. Red, magnetic beads functionalized with Atto-Biotin. c(beads) = 1 mg/mL. White rectangle, region of interest (ROI). Dashed line, B_{max}= point of extraction. t_1, droplet before magnet. t_2, droplet at point of extraction. t_3, droplet after point of extraction. Images are overlays of multiple pictures recorded with a G-2A and a Cy5 fluorescence filter. The droplet solution was colored with a green dye (Cy3). (b,e) Illustration of (a,d). Blue, aqueous phase. Gray, carrier fluid. Brown, magnetic beads. N, magnetic north. S, magnetic south. Red arrow, magnetic force. Black arrow, capillary force. t_{1-3}, position of the same droplet at different times. (c,f) Signal intensity in the ROI (white rectangles) over time for five droplets. Black, mean gray value. Blue, enveloping curve. Red, linear regression of the accumulated signal.

For large amounts of beads, a nonlinear signal increase is observed (see Supporting Information, **Figure S-2**). Thus, a periodical release of the accumulated beads by removing the magnets from the channel is important. The ability to extract low amounts of beads minimizes the danger of shading and of the obstruction of the channel by the beads. The bead extraction efficiency was therefore a major limiting factor and a key concern for optimization.

Sequential measurements. To increase the throughput, we explored the feasibility of sequential measurements. First, droplets containing 100 µg/mL streptavidin-coated beads were generated in reverse direction to flow 1 (as described above). The droplet volume was estimated to be approximately 23 nL (Supporting Information, **Figure S-3**). To mimic several consecutive samples, we produced a dilution series with 11 concentrations of Atto-Biotin in PBST (c = 0−10,000 pg/mL, **Figure 4 a**).

The samples were added sequentially at the first T−junction to the droplets with the bead dispersion (details in Supporting Information, **Figure S-1**) resulting in about 50 droplets per sequence with a volume of approximately 43 nL. PBST was added at the second T-junction, resulting in a droplet volume of approximately 63 nL. We let the droplets incubate while moving them through a series of horizontal coils to the magnetic trap. During the accumulation of the beads in the magnetic trap, we observed a linear signal increase for each tested concentration (**Figure 4a**). At the end of each sequence, the signal returned to the baseline upon each trap opening, indicative of a full release of the beads from the magnetic trap.

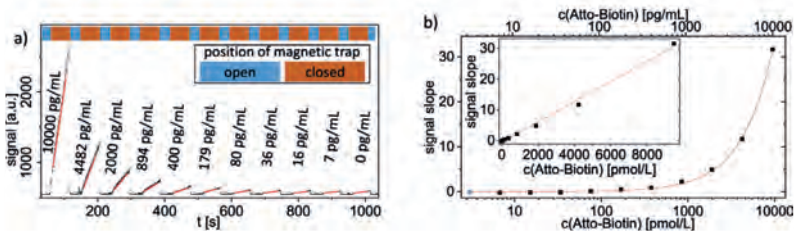

Figure 4. Sequential measurements of an Atto-Biotin dilution series. (a) Sequential measurements of 11 Atto-Biotin concentrations (0−10,000 pg/mL). The position of the magnetic trap is indicated in blue (open) and brown (closed). n = 1. (b) Signal slopes plotted against the different target concentrations. c(beads) = 100 µg/mL. Red, sigmoidal fit (R^2 > 0.99). Blue data point, negative control (0 ng/mL), added as the lowest value of the dilution series. Insert: linear scale. Red, linear fit (R^2 > 0.99).

The signal slopes for the sequences increased proportionally with the target concentrations (R^2 > 0.99, **Figure 4b**, insert). In logarithmic plots, we used sigmoidal fits to describe the signal slope increase, as proposed earlier by Holstein et al.[24] In repeated bead accumulations, the homogeneous distribution of the magnetic beads across the droplets was tested (Supporting Information, bead distribution CV_{slopes} = 5%, **Figure S-4a**; inter-assay CV_{slopes} = 8%, **Figure S-4b**).

In summary, the linear slopes of the signals, the low signal variability, and the correlation with the different Atto-Biotin concentrations (**Figure 4**) indicate that droplet generation, reagent addition, and Atto-Biotin binding to the beads were accurate and reproducible in sequential measurements. Thus, we extended our system by the sequential measurement option to increase the throughput and to ensure uniform conditions for all samples of a series.

Optimization of the LoD. We next evaluated and optimized the sensitivity of the microfluidic system. According to Armbruster and Pry,[26] we determined the LoD as the background signal +4 × standard deviation (SD). Thus, the LoD can be improved by reducing the background signal and/ or its SD. Two major system-immanent factors were considered to increase the signal-to-background ratio: (i) light source, whose emission spectrum determines the fluorescence intensity by exciting the fluorescent dye and the background signal stemming from the magnetic beads and

(ii) the beads as emitters of background signal, e.g., through autofluorescence and/or light scattering.

A good spectral overlap between the emission spectrum of the light source with the absorption spectrum of the fluorescent dye is a prerequisite for high fluorescence intensity. So far, our system was equipped with a metal halide lamp in combination with a Cy5 excitation filter which has its emission maximum at 593 nm (Supporting Information, **Figure S-5**). To increase the overlap, we replaced the metal halide lamp with an LED light source that has an emission maximum at 636 nm. The integral was 6 times higher for the LED in the range of the Cy5 filter and overlapped substantially with the absorption spectrum of the fluorescent dye (Atto-647N-Biotin, maximum absorption at 646 nm). Consequently, the LED lamp increased the slope of the dose response curve by a factor of 14. Furthermore, the signal/background ratio increased from the background for lower target concentrations. As a consequence, the use of the LED lamp improved the sensitivity of our system by more than 1 order of magnitude and reduced the LoD from about 100 pg/mL to approximately 8 pg/mL (Supporting Information, **Figure S-5**).

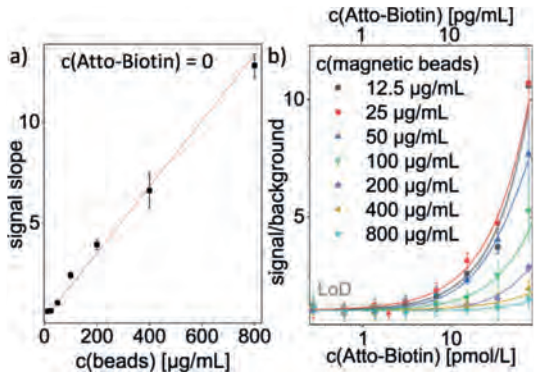

Figure 5. Enhancing the LoD. (a) Background signal measured at c(Atto-Biotin) = 0 pg/mL for a bead dilution series (800−12.5 µg/mL). Red line, linear fit (R^2 = 0.97). Data points, mean ± SD n = 3. (b) Signal/background ratio for an Atto-Biotin dilution series (0−80 and 0−400 pg/mL for c(beads) > 100 µg/mL) at different bead concentrations. Solid lines, sigmoidal fits. Dashed, LoD at c(beads) = 25 µg/mL. Red arrow, lowest detectable concentration (2 pmol/L for c(beads) = 25 µg/mL). The section of the diagram was chosen such that the differences in the area of the LoD are visible. Data for c(magnetic beads) = 100 µg/mL are reproduced from (b) (LED). Data points, mean ± SD n = 3.

To address the beads as emitters of background signal (ii), we hypothesized that lower bead concentrations reduce the background signal. Therefore, we tested whether down titration of the magnetic beads lowers the LoD. Indeed, it was found that the magnetic bead concentration positively correlates with the background signal (**Figure 5a**). When evaluating the signal/background ratio, there appears to be an improvement at lower bead concentrations (**Figure 5b**). From this, an optimal signal/background ratio could be determined at c(beads) = 25 µg/mL. At this bead concentration, the lowest analyte concentration (2 pg/mL) can be detected at the

LoD. Reducing or increasing the bead concentration results in an increase in the analyte concentration at the LoD, suggesting an ideal bead concentration of 25 µg/mL. In keeping with our findings, Teste et al.[16] have shown earlier with a comparable microfluidic setup that down titration of the bead concentration enhances the detection sensitivity. However, this study did not assess magnetic bead concentrations below 1 mg/mL, possibly because their system could not efficiently extract the magnetic beads at lower concentrations. Thus, the extraction efficiency of our system at low magnetic bead concentrations is key to enhance its sensitivity beyond earlier approaches. The capacity to detect the analyte is maintained as long as there are sufficient binding sites available.

Proof of Concept: Sandwich immunoassays. Next, we tested the performance of our microfluidic concept with sandwich immunoassays, targeting proteins of biomedical relevance. We conducted assays for (i) the inflammatory marker interleukin 6 (IL−6)[27,28] and (ii) the metabolic master regulator mTOR (mammalian target of rapamycin), which is the central hub of the oncogenic phosphoinositide-3-kinase (PI3K)−mTOR network.[29,30] Recombinant IL-6 and mTOR were detected with antibody pairs directed against different regions of the target proteins. As the affinity of an antibody to its target is typically lower than for streptavidin−biotin (10^{-9}−10^{-12} mol/L for antibodies[31] versus 10^{-13} mol/L for streptavidin-biotin[23]), the incubation time was increased from 13.5 to 27 min. Furthermore, the glass capillaries were partially hydrophobized with trichloro(1H,1H,2H,2H-perfluorooctyl) silane, as wetting of the capillary by the aqueous solution increases the risk of non-specific protein adsorption. In the area of bead extraction, the capillaries remained hydrophilic to maintain the required wetting properties for efficient bead extraction.

The microfluidic assays were set up as pictured in **Figure 1**. First a droplet train was produced, containing magnetic beads coated with capture antibody. Samples with different concentrations of recombinant target protein were added at the first T-junction. At the second T-junction, a solution of the fluorophore-labelled antibody (detection antibody) was added. We observed for both IL-6- and mTOR-directed immunoassays a positive correlation between the signal slope and the analyte concentration (IL-6: R^2 = 0.98, mTOR: R^2 = 0.93, **Figure 6**, red lines). The low molecular weight protein IL-6 (20.3 kDa) was detectable at concentrations of 25 pmol/L (510 pg/mL, **Figure 6a**) or higher, while the high molecular weight protein mTOR (289 kDa) was detectable at a minimum concentration of 800 pmol/L (230 ng/mL) (**Figure 6b**). Comparable microfluidic platforms with nanoliter-reaction compartments for protein assays showed concentrations at the LoDs of 40 pmol/L (TSH-hormone, 13 kDa)[14] and 500 pmol/L (amyloid-ß peptide, 4−4.5 kDa)[18]. Thus, our microfluidic setup with IL-6, which is comparable in size to TSH-hormone and amyloid-ß peptide (20.3 versus 13 and 4.5 kDa, respectively), was at least 1.5−10 times more sensitive than the earlier approaches (25 versus 40 and 500 pmol/L for TSH-hormone and amyloid- ß peptide respectively).[14,18]

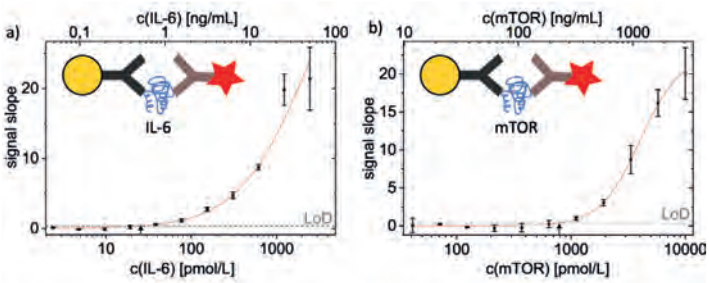

Figure 6. Microfluidic detection of proteins by a sandwich immunoassay. (a) Detection of an IL-6 dilution series (0−50 ng/mL). c(beads) = 50 µg/mL. Red, sigmoidal fit (R^2 = 0.98). Dashed line, LoD. Arrow, intersection of the sigmoidal fit and the LoD indicating the lowest detectable concentration (c(IL-6) = 25 pmol/L). Data points, mean ± SD n = 3. (b) Detection of an mTOR dilution series (0−2889 ng/mL). c(beads) = 100 µg/mL. Red, sigmoidal fit (R^2 = 0.93). Arrow, intersection of the sigmoidal fit and the LoD indicating the lowest detectable concentration (c(mTOR) = 800 pmol/L). Data points, mean ± SD n = 3.

To the best of our knowledge, we present here the first nanoliter droplet-based microfluidic assay for mTOR. Several inherent properties of this protein can make it difficult to evaluate it in a microfluidic setup. It has been suggested that precipitation, aggregation, and/or adsorption impede the detection of proteins in microfluidics.[32] mTOR exhibits a very high molecular weight, and is membrane-associated.[33–35] Such properties often result in poor protein solubility, which likely explains the comparably high concentration required at the LoD for mTOR seen in this study (800 pmol/L as compared to 25 pmol/L for IL-6). Further optimization may allow lowering the detectable concentration at the LoD in the future.

Conclusion and outlook

We present here a microfluidic platform for magnetic beadbased sandwich immunoassays in nanoliter droplets. The platform enables sequential measurements, which are key for medium and high throughput applications. By introducing a hydrophilic channel in the area of bead extraction, we achieve reliable bead extraction for bead concentrations down to 12.5 µg/mL. Earlier approaches for heterogeneous assays reported bead extraction for concentrations ≥ 1 mg/mL[14,16–18,22]. Thus, with this setup, the performance was improved by 2 orders of magnitude. We also show the importance of working at the optimal bead concentration, as concentrations above or below this optimum dramatically reduce the sensitivity of the system. In a proof of concept, we showed that the present platform is compatible with immunoassays. The concentration at the LoD of the low molecular weight protein IL-6 improves by a factor of 1.5−10 compared to values reported earlier for comparable microfluidic setups.[14,17]

Conventional sandwich immunoassays, such as ELISAs on microtiter plates typically require sample and reagent volumes of 50 µL per technical replicate,

intermediate washing steps and 2−3 incubation steps of 1−2 hours each.[36] With the miniaturized analysis-platform presented here, the incubation time is reduced from several hours down to 27 minutes. To generate approximately 50 reaction compartments at the nanoliter scale, 2 µL of sample, 1 µL of magnetic bead-dispersion (c = 25−100 µg/mL) and 1 µL of detection antibody-solution (c = 1 µg/mL) per sequence are sufficient. Thus, the volumes of samples and reagents are reduced by factors of 25−50. In summary, the transfer of heterogeneous immunoassays to a two-phase microfluidic system reduces the sample consumption by a factor of at least 25 while producing 50 times more technical replicates than conventional immunoassays.[36]

In the future, we envision to further develop our microfluidic platform for systems studies[37–39] to acquire data series such as time courses with high resolution and accuracy and with high numbers of biological and technical replicates. This will enhance the statistical reliability of data for computational modeling. Furthermore, we anticipate that our platform presents strong advantages where sample and/or reagent volumes are limiting and high throughput is required, such as in biomedical applications with patient material. The nanoliter reaction chambers will allow to quantify proteins from low volumes of patient samples such as tissue or liquid biopsies. Furthermore, the high degree of parallelization enables higher accuracy, reproducibility, and time-efficiency than established immunodetection methods. This is important for clinical applications that are time sensitive and require high accuracy.

In summary, the microfluidic platform presented here combines an innovative approach for efficient bead extraction from nanoliter droplets and enables sequential sandwich immunoassays. This opens new avenues for the implementation of microfluidics in the systems biology and medicine.

Notes

The authors declare no competing financial interest.

Acknowledgments

We thank Birgit Holzwarth for supporting us in this interdisci-plinary project, Holger Frey for programming the Arduino microcontroller and Nathan Bentley for his help in the revision process. We gratefully acknowledge funding from the Deutsche Forschungsgemeinschaft (DFG, German Research Foundation) – project numbers RU 489/31-1 and TH 1358/3-1. KT acknowledges support from the MESI-STRAT project (grant agreement No. 754688) and the PoLiMeR Innovative Training Network (Marie Skłodowska-Curie grant agreement No. 812616) which both have received funding from the European Union's Horizon 2020 research and innovation programme. KT is recipient of the Research Award of the German Tuberous Sclerosis Foundation 2017 and acknowledges support from the German TS Foundation and the Stichting TSC Fonds.

References

(1) Shang, L.; Cheng, Y.; Zhao, Y. Emerging Droplet Microfluidics. Chem. Rev. 2017, 117 (12), 7964–8040. https://doi.org/10.1021/acs.chemrev.6b00848.

(2) Mashaghi, S.; Abbaspourrad, A.; Weitz, D. A.; van Oijen, A. M. Droplet Microfluidics: A Tool for Biology, Chemistry and Nanotechnology. TrAC Trends in Analytical Chemistry 2016, 82, 118–125. https://doi.org/10.1016/j.trac.2016.05.019.

(3) Seemann, R.; Brinkmann, M.; Pfohl, T.; Herminghaus, S. Droplet Based Microfluidics. Rep. Prog. Phys. 2012, 75 (1), 016601. https://doi.org/10.1088/0034-4885/75/1/016601.

(4) T. Guo, M.; Rotem, A.; A. Heyman, J.; A. Weitz, D. Droplet Microfluidics for High-Throughput Biological Assays. Lab on a Chip 2012, 12 (12), 2146–2155. https://doi.org/10.1039/C2LC21147E.

(5) Fidalgo, L. M.; Whyte, G.; Bratton, D.; Kaminski, C. F.; Abell, C.; Huck, W. T. S. From Microdroplets to Microfluidics: Selective Emulsion Separation in Microfluidic Devices. Angewandte Chemie 2008, 120 (11), 2072–2075. https://doi.org/10.1002/ange.200704903.

(6) Trivedi, V.; Doshi, A.; Kurup, G. K.; Ereifej, E.; Vandevord, P. J.; Basu, A. S. A Modular Approach for the Generation, Storage, Mixing, and Detection of Droplet Libraries for High Throughput Screening. Lab Chip 2010, 10 (18), 2433–2442. https://doi.org/10.1039/C004768F.

(7) Song, H.; Chen, D. L.; Ismagilov, R. F. Reactions in Droplets in Microfluidic Channels. Angewandte Chemie International Edition 2006, 45 (44), 7336–7356. https://doi.org/10.1002/anie.200601554.

(8) Shembekar, N.; Chaipan, C.; Utharala, R.; A. Merten, C. Droplet-Based Microfluidics in Drug Discovery, Transcriptomics and High-Throughput Molecular Genetics. Lab on a Chip 2016, 16 (8), 1314–1331. https://doi.org/10.1039/C6LC00249H.

(9) Serra, M.; Ferraro, D.; Pereiro, I.; Viovy, J.-L.; Descroix, S. The Power of Solid Supports in Multiphase and Droplet-Based Microfluidics: Towards Clinical Applications. Lab on a Chip 2017, 17 (23), 3979–3999. https://doi.org/10.1039/C7LC00582B.

(10) Rendl, M.; Brandstetter, T.; Rühe, J. Solid-Phase Extraction in Segmented Flow. Langmuir 2014, 30 (43), 12804–12811. https://doi.org/10.1021/la502645z.

(11) Lombardi, D.; Dittrich, P. S. Droplet Microfluidics with Magnetic Beads: A New Tool to Investigate Drug–Protein Interactions. Analytical and Bioanalytical Chemistry 2011, 399 (1), 347–352. https://doi.org/10.1007/s00216-010-4302-7.

(12) Brouzes, E.; Kruse, T.; Kimmerling, R.; H. Strey, H. Rapid and Continuous Magnetic Separation in Droplet Microfluidic Devices. Lab on a Chip 2015, 15 (3), 908–919. https://doi.org/10.1039/C4LC01327A.

(13) Gao, R.; Cheng, Z.; J. deMello, A.; Choo, J. Wash-Free Magnetic Immunoassay of the PSA Cancer Marker Using SERS and Droplet Microfluidics. Lab on a Chip 2016, 16 (6), 1022–1029. https://doi.org/10.1039/C5LC01249J.

(14) Ali-Cherif, A.; Begolo, S.; Descroix, S.; Viovy, J.-L.; Malaquin, L. Programmable Magnetic Tweezers and Droplet Microfluidic Device for High-Throughput Nanoliter Multi-Step Assays. Angewandte Chemie International Edition 2012, 51 (43), 10765–10769. https://doi.org/10.1002/anie.201203862.

(15) Long, Z.; Shetty, A. M.; Solomon, M. J.; Larson, R. G. Fundamentals of Magnet-Actuated Droplet Manipulation on an Open Hydrophobic Surface. Lab Chip 2009, 9 (11), 1567–1575. https://doi.org/10.1039/b819818g.

(16) Teste, B.; Ali-Cherif, A.; Viovy, J. L.; Malaquin, L. A Low Cost and High Throughput Magnetic Bead-Based Immuno-Agglutination Assay in Confined Droplets. Lab on a Chip 2013, 13 (12), 2344. https://doi.org/10.1039/c3lc50353d.

(17) Ferraro, D.; Champ, J.; Teste, B.; Serra, M.; Malaquin, L.; Viovy, J.-L.; de Cremoux, P.; Descroix, S. Microfluidic Platform Combining Droplets and Magnetic Tweezers: Application to HER2 Expression in Cancer Diagnosis. Sci Rep 2016, 6. https://doi.org/10.1038/srep25540.

(18) Mai, T. D.; Ferraro, D.; Aboud, N.; Renault, R.; Serra, M.; Tran, N. T.; Viovy, J.-L.; Smadja, C.; Descroix, S.; Taverna, M. Single-Step Immunoassays and Microfluidic Droplet Operation: Towards a Versatile Approach for Detection of Amyloid-β Peptide-Based Biomarkers of Alzheimer's Disease. Sensors and Actuators B: Chemical 2018, 255, 2126–2135. https://doi.org/10.1016/j.snb.2017.09.003.

(19) Tabeling, P. Introduction to Microfluidics; Oxford University Press: Oxford, U.K. ; New York, 2005.

(20) Rendl, M.; Brandstetter, T.; Rühe, J. Time-Resolved Analysis of Biological Reactions Based on Heterogeneous Assays in Liquid Plugs of Nanoliter Volume. Anal. Chem. 2013, 85 (20), 9469–9477. https://doi.org/10.1021/ac401752j.

(21) M. Fidalgo, L.; Abell, C.; S. Huck, W. T. Surface-Induced Droplet Fusion in Microfluidic Devices. Lab on a Chip 2007, 7 (8), 984–986. https://doi.org/10.1039/B708091C.

(22) Schönberg, J.-N.; Brandstetter, T.; Rühe, J. Particle Extraction in Plug-Based Microfluidics. Procedia Engineering 2015, 120, 96–99. https://doi.org/10.1016/j.proeng.2015.08.574.

(23) DeChancie, J.; Houk, K. N. The Origins of Femtomolar Protein−Ligand Binding: Hydrogen-Bond Cooperativity and Desolvation Energetics in the Biotin−(Strept)Avidin Binding Site. J. Am. Chem. Soc. 2007, 129 (17), 5419–5429. https://doi.org/10.1021/ja066950n.

(24) Holstein, C. A.; Griffin, M.; Hong, J.; Sampson, P. D. Statistical Method for Determining and Comparing Limits of Detection of Bioassays. Anal. Chem. 2015, 87 (19), 9795–9801. https://doi.org/10.1021/acs.analchem.5b02082.

(25) Fong, Y.; Yu, X. Transformation Model Choice in Nonlinear Regression Analysis of Fluorescence-Based Serial Dilution Assays. Statistics in Biopharmaceutical Research 2016, 8 (1), 1–11. https://doi.org/10.1080/19466315.2015.1093019.

(26) Armbruster, D. A.; Pry, T. Limit of Blank, Limit of Detection and Limit of Quantitation. Clin Biochem Rev 2008, 29 (Suppl 1), S49–S52.

(27) Heinrich, P. C.; Behrmann, I.; Haan, S.; Hermanns, H. M.; Müller-Newen, G.; Schaper, F. Principles of Interleukin (IL)-6-Type Cytokine Signalling and Its Regulation. Biochem J 2003, 374 (Pt 1), 1–20. https://doi.org/10.1042/BJ20030407.

(28) Mansell, A.; Jenkins, B. J. Dangerous Liaisons between Interleukin-6 Cytokine and Toll-like Receptor Families: A Potent Combination in Inflammation and Cancer. Cytokine & Growth Factor Reviews 2013, 24 (3), 249–256. https://doi.org/10.1016/j.cytogfr.2013.03.007.

(29) Navas, P. R.; Thedieck, K. Differential Control of Ageing and Lifespan by Isoforms and Splice Variants across the MTOR Network. Essays In Biochemistry 2017, 61 (3), 349–368. https://doi.org/10.1042/EBC20160086.

(30) Saxton, R. A.; Sabatini, D. M. MTOR Signaling in Growth, Metabolism, and Disease. Cell 2017, 168 (6), 960–976. https://doi.org/10.1016/j.cell.2017.02.004.

(31) Landry, J. P.; Ke, Y.; Yu, G.-L.; Zhu, X. D. Measuring Affinity Constants of 1450 Monoclonal Antibodies to Peptide Targets with a Microarray-Based Label-Free Assay Platform. J. Immunol. Methods 2015, 417, 86–96. https://doi.org/10.1016/j.jim.2014.12.011.

(32) Roach, L. S.; Song, H.; Ismagilov, R. F. Controlling Nonspecific Protein Adsorption in a Plug-Based Microfluidic System by Controlling Interfacial Chemistry Using Fluorous-Phase Surfactants. Anal. Chem. 2005, 77 (3), 785–796. https://doi.org/10.1021/ac049061w.

(33) De Cicco, M.; Abd Rahim, M. S.; Dames, S. A. Regulation of the Target of Rapamycin and Other Phosphatidylinositol 3-Kinase-Related Kinases by Membrane Targeting. Membranes (Basel) 2015, 5 (4), 553–575. https://doi.org/10.3390/membranes5040553.

(34) Betz, C.; Hall, M. N. Where Is MTOR and What Is It Doing There? J Cell Biol 2013, 203 (4), 563–574. https://doi.org/10.1083/jcb.201306041.

(35) Yuan, H.-X.; Guan, K.-L. The SIN1-PH Domain Connects MTORC2 to PI3K. Cancer Discov 2015, 5 (11), 1127–1129. https://doi.org/10.1158/2159-8290.CD-15-1125.

(36) Crowther, J. R. The ELISA Guidebook; Walker, J. M., Series Ed.; Methods in Molecular Biology; Humana Press: Totowa, NJ, 2009; Vol. 516. https://doi.org/10.1007/978-1-60327-254-4.

(37) Dalle Pezze, P.; Sonntag, A. G.; Thien, A.; Prentzell, M. T.; Gödel, M.; Fischer, S.; Neumann-Haefelin, E.; Huber, T. B.; Baumeister, R.; Shanley, D. P.; et al. A Dynamic Network Model of MTOR Signaling Reveals TSC-Independent MTORC2 Regulation. Sci Signal 2012, 5 (217), ra25. https://doi.org/10.1126/scisignal.2002469.

(38) Dalle Pezze, P.; Ruf, S.; Sonntag, A. G.; Langelaar-Makkinje, M.; Hall, P.; Heberle, A. M.; Razquin Navas, P.; van Eunen, K.; Tölle, R. C.; Schwarz, J. J.; et al. A Systems Study Reveals Concurrent Activation of AMPK and MTOR by Amino Acids. Nat Commun 2016, 7, 13254. https://doi.org/10.1038/ncomms13254.

(39) Heberle, A. M.; Razquin Navas, P.; Langelaar-Makkinje, M.; Kasack, K.; Sadik, A.; Faessler, E.; Hahn, U.; Marx-Stoelting, P.; Opitz, C. A.; Sers, C.; et al. The PI3K and MAPK/P38 Pathways Control Stress Granule Assembly in a Hierarchical Manner. Life Sci Alliance 2019, 2 (2). https://doi.org/10.26508/lsa.201800257.

Supplementary Information for

Chapter 3

Breaking the interface: efficient extraction of magnetic beads from nanoliter-droplets for automated sequential immunoassays

Table of content

Find a movie, demonstrating the operation principle, as additional supporting information online. https://pubs.acs.org/doi/10.1021/acs.analchem.0c00187.

Reagents and materials.

Assay components and reagents. Streptavidin coated superparamagnetic beads were obtained from Invitrogen GmbH (Dynabeads MyOne Streptavidin T1, #65601, US). Fluorescence-labeled biotin was obtained from Sigma Aldrich (Atto-647N-Biotin, #93606, Germany). The following antibodies were used as capture antibodies: biotinylated anti-IL-6 antibody (antibody raised in goat against human IL-6, residues M1-M212, #BAF206, R&D, US) and biotinylated anti-mTOR antibody (Clone 3G6[1], antibody raised in rat against human mTOR, residues T221-I260). The following Alexa Fluor 647 labeled antibodies were used as detection antibodies: anti-IL-6 antibody (Clone 6708, antibody raised in mouse, #NBP2-59771AF647, Novus, US) and anti-mTOR antibody (Clone 7C10, raised in rabbit against residues surrounding S2481 of human mTOR, #5048, Cell Signaling, US). Detection antibodies were used at a concentration of 1 µg/mL. For sandwich immunoassays, recombinant human IL-6 (E. coli-derived, residues P29-M212, #Q75MH2, R&D, US) and recombinant human mTOR (HEK293T-derived, #TP320457, OriGene Technologies, US) were used. All aqueous solutions were based on a phosphate buffered saline (#P4417, Sigma-Aldrich, US) containing 0.1 % (v/v) Tween 20 (#P9416-100, Sigma-Aldrich, US), referred to as PBST.

Fluidic setup. Fluorinated ethylene propylene (FEP) tubing (inner diameter 0.25 mm, outer diameter 1.60 mm, #2001001, PRO LIQUID GmbH, Germany) was used to build the microfluidic system. The tubes were connected by CTFE T-junctions and union fittings (microvolume connector - 1/16” - 0.25mm bore, VICI AG International, MT1CKF & MU1CKF, MACHEREY-NAGEL GmbH, Germany). The fluorocarbon oils FC-3283 (perfluorotripropylamine) and FC-43 (perfluorotributylamine) were used as the water immiscible carrier oil (3M, #FL-0008-HP and #FL-0006-HP, Iolitec, US). Precise and programmable flow was enabled by neMESYS 290 N syringe-pumps (#A3921000132, Cetoni GmbH, Germany) equipped with glass-syringes (500 µL PTFE 1/4-28UNF, 3010387 and 1.0 mL PTFE 1/4-28UNF, 3010307, SETonic, Germany).

Magnetic separation setup. The magnetic trap consisted of two neodymium magnets (15x4x4 mm, 1.35 T, NdFeB, # Q-15-04-04-MN, WebCraft GmbH, Germany) on both sides of either FEP tubing or a glass capillary (2 µL minicaps, end to end, #L919.2, Hirschmann Laborgeräte GmbH & Co. KG, Germany). The magnets were actuated by servomotors (Top-Line RS2 MG/BB, modelcraft, #205111-62, Conrad Electronic SE, Germany) controlled by a programmable Arduino UNO microcontroller (DIP Version ATMega328, EAN: 9783645652803, Conrad Electronic SE, Germany) with an Adafruit prototyping shield (# EXP-R15-552, EXP GmbH, Germany). The magnetic field lines were simulated with the software Finite Element Method Magnetics (version 4.2).

Optical setup. To detect the fluorescent signal, we used an inverted microscope (Nikon TS 100, #203537, Nikon GmbH, Germany) equipped with 2x (Nikon Plan Achromat UW, MRL00022, Nikon GmbH, Germany) or 4x (Nikon Plan Fluor, MRH00040, Nikon GmbH, Germany) objectives and a CMOS camera (Orca Flash 4.0 - C13400, #300556, Hamamatsu Photonics K.K., Japan) and Hokawo - Imaging Software (v2.10, Hamamatsu Photonics K.K., Japan) and NIS Elements BR (v5.02.01, Nikon GmbH, Germany). A metal halide (Intensilight C-HGFI, #684409, Nikon GmbH, Germany) or a LED light source (SOLA SE II, #14904, LUMENCOR, USA) were used with Cy5 (Cy5 ET Filter Set, #F46-006, AHF analysentechnik AG, Germany) or G-2A (G-2A, MBE45500, Nikon GmbH, Germany) fluorescence filters.

Microfluidic procedure

General procedure. The setup for sandwich immunoassays in nanoliter-droplets is shown schematically in the main paper, **Figure 1**. The procedure consisted of the following steps: (*i) Droplet generation, reverse to flow 1*. The droplets were generated by adding through flow 2 a dispersion of beads with bound capture antibodies (flow rate of 6.5 µL/min), reverse to flow 1 containing carrier fluid (flow rate of -30 µL/min). For the setup with only flow 1 and 2, the Hagen-Poiseuille-Law predicts a negative pressure of 368 mbar for FC-43 (dynamic viscosity $\eta = 4.7$ mPa · s) and 110 mbar for FC-3283 ($\eta = 1.4$ mPa · s). Thus, flow 3 containing carrier fluid (flow rate 30 µL/min) compensated this to a slight overpressure of 23 mbar (FC-3283). For homogeneous bead distribution across the plugs, careful homogenization and fast processing (<3 min) of the bead containing solution into droplets is needed to prevent magnetic particle sedimentation. *(ii) Addition of further reagents.* The bead containing droplets (flow 1) moved at a constant flow rate of 5 µL/min. The flow rates of the solutions added at the T-junctions were 1 µL/min for flow 2 containing the analyte; and 1 µL/min for flow 3, containing fluorophore-labeled detection antibodies, or PBST (in the case of Atto-647N-Biotin experiments). For later sandwich immunoassays all flow speeds for addition of further reagents were divided by two. *(iii) Incubation at constant flow rates* (Atto-647N-Biotin, 7 µl/min; sandwich immunoassays, 3.5 µL/min). The incubation time (Atto-647N-Biotin, 13.5 min; sandwich immunoassays, 27 min) is thereby determined by the flow speed and the distance (147 cm) between the second merging point and the magnetic trap (point of detection). *(iv) Magnetic bead extraction and detection of the fluorescent signal over time at the magnetic trap.* The magnetic beads of each sequence were sequentially accumulated in the magnetic trap. Therefore, opening and closing of the magnetic trap was synchronized with the fluidic workflow. For Atto-647NBiotin experiments: 55 s extraction at 7 µL/min; for sandwich immunoassays: 110 s extraction at 3.5 µL/min. The fluorescence signal was thereby recorded with an inverted microscope (Atto-647NBiotin, 3.3 frames/s; sandwich immunoassays 2 frames/s). After opening the magnetic trap, the release

of the beads was supported by an additional wash-flow (**Figure 1**, flow 4, 6µL, 60 µL/min).

Sequential measurements. In comparison to the measurement of single samples, sequential measurements required a more complex coordination of the flows. For sequential measurements, multiple samples were added to a train of droplets containing beads at the first T-junction in iterative steps (**Figure S-1a**). In detail, the procedure consisted of the following steps:

(1) Dispensing of a fraction of the sample into the main channel (flow 1: V = 0.5 µL, v = 1 µL/min; flow 2: V = 0 µL, v = 0 µL/min).

(2) Addition of the sample to the train of droplets containing magnetic beads (flow 1: V = 1 µL, v = 1 µL/min; flow 2: V = 5 µL, v = 5 µL/min).

(3) Release of non-used sample and spacer carrier oil from flow 2 (flow 1: V = 3 µL, v = 6 µL/min; flow 2: V = 0 µL, v = 0 µL/min).

Step 2 and 3 were repeated until all samples were added sequential to the train of droplets. The resulting flow speed remained thereby constantly at 6 µL/min. After the merging of all samples with the droplets containing magnetic beads, the detection antibody was added at the second T-junction with a constant flow rate of 1 µl/min (**Figure S-1b**). The constant flow speed leads to a uniform incubation time for all droplets before the assay-product is detected in the magnetic trap. For the sandwich immunoassays, we reduced the flow speeds by a factor of two to increase the time of incubation. The overall setup with the process for sequential measurements is summarized in **Figure S-1c**. In flow 2, the samples are separated by carrier fluid. Between the sample droplets - generated by flow 2, flow 3 creates droplets serving as spacers between the samples (**Figure S-1**, red droplets). As these contain the undiluted solution of detection antibody, they appear bright in the fluorescence microscope and can be a helpful orientation for synchronizing the flow pattern to the magnetic trap schedule.

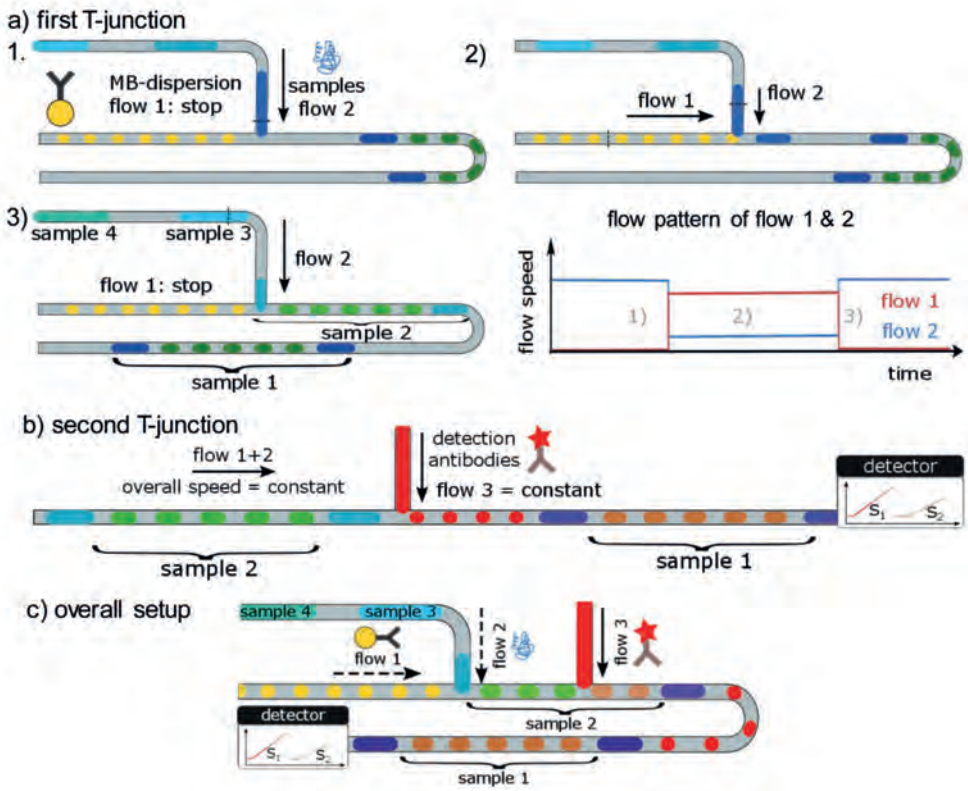

Figure S-1: Schematic illustration of the flow pattern for sequential measurements. (a) Multiple samples (shades of blue) are added to a droplet train containing magnetic beads (yellow) in three iterative steps (1-3) at the first T-junction. The flow speeds of flow 1 and flow 2 are regulated in an opposite manner. Thus, the overall flow-speed is constant. Green, sample + beads. Black dashed line, target of the respective dispensing-step. (b) The detection antibody (red) is added to the droplet train containing samples and beads (green) at the second T-junction. Blue, sample. Brown, sample + beads + detection antibody. Purple, sample + detection antibody. (c) The overall setup, including both T-junctions.

Accumulation of beads

Assuming that each droplet contributes the same amount of beads with the same amount of fluorescent dye on their surface, a linear increase of the detected signal would be expected. In order to investigate this, a droplet train containing beads (c = 100µg/mL) pre-functionalized with Atto-647N-Biotin (c = 2 ng/mL) was created by adding the aqueous phase (flow speed, 6.5 µl/min) to the carrier-fluid (flow speed, 30 µL/min). At the point of detection the magnetic beads were accumulated at a flow speed of 7 µL/min. The signal increased in a linear manner over 60 s in good agreement with the linear fit (**Figure S-2a**, R^2 = 0.997). Thus, we conclude that the magnetic beads were distributed homogenously over the droplets.

We observed a deviation of the linearity for longer extraction-times (1 - 5 min) and/or large amounts of beads (**Figure S-2b**). This could be due to shading, bleaching and/or the loss of beads due to the increasing obstruction of the channel. Thus, for remaining in the linear area, we adjusted the extraction time for the respective flow speeds - 55 s extraction at 7 µL/min for Atto-647N-Biotin experiments, 110 s extraction at 3.5 µL/min for sandwich immunoassays). The ability to accumulate low concentrations of beads expands thereby the window of operation to longer extraction times.

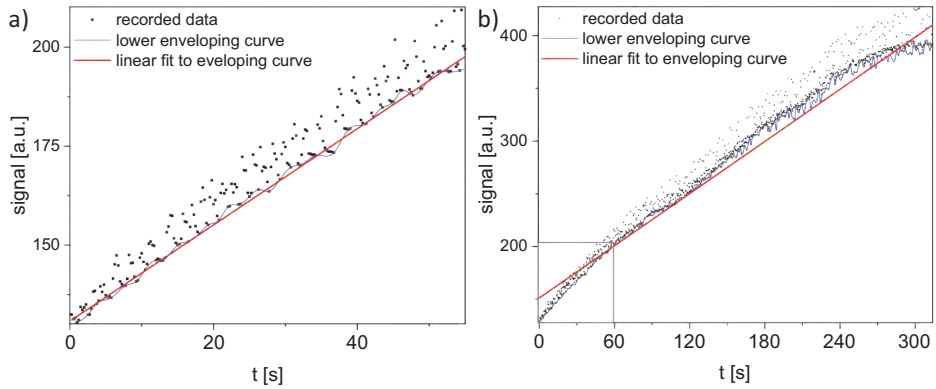

Figure S-2: Signal increase over time for accumulated functionalized beads. (a) Signal increase over 60 s. Magnification of data shown in (b, gray insert). c(beads) = 100 µg/mL. Black points, recorded data. Blue line, enveloping curve. Red line, linear fit to enveloping curve (R^2 = 0.997). The lower enveloping curve separates the relevant data points from the noise. The linear regression matches the lower enveloping curve. (b) Signal increase over time by accumulation of beads functionalized with Atto-647N-Biotin (c = 2 ng/mL). c(beads) = 100 µg/mL. Black points, recorded data. Blue line, enveloping curve, Red line, linear fit to enveloping curve (R^2 = 0.980). The gray insert contains the area magnified in (a).

When a plug passes the ROI, the fluorescence signal reaches a local maximum (compare **Figure 4 e**) and **f**) – main paper). This consists of the signal of the accumulated beads and the unbound fluorophores in solution. Since only the signal of the accumulated beads represents the relevant signal, the maxima appear as noise. To bypass the influence of these peaks, the data points representing the stepwise signal-increase of the accumulated beads can be separated manually from the noise. The same effect is achieved by plotting the *lower envelope* (see also **Figure 4 f**) – main paper). This makes the evaluation of the data more efficient and avoids a biased selection. In the Origin Lab handbook, this data processing step is described as following for the upper enveloping curve: "*Envelope* is a curve enveloping the source data. It is tangent to every peak in the source dataset. Origin obtains the upper, lower, or both envelopes of the source data by applying a local maximum method combined with a cubic spline interpolation."[2]

Volume of the droplets

To measure the volume of the aqueous droplets before and after the merging steps, we produced the droplets as described in the main paper (flow 1: -30 µL/min, flow 2: 6.5 µL/min, flow 3: 30 µL/min). Then, we merged these droplets at the T-junctions with the aqueous solutions of flow 2 and 3 (flow 1: 5 µL/min, flow 2: 1 µL/min, flow 3: 1 µL/min) and observed the droplets at the different positions of the fluidic setup with the microscope. We derived the volumes from the average length of the droplets by assuming a shape composed of a cylinder and two hemispheres. The volume of the initial droplets (**Figure S-3 I**) was calculated to 23.1 ± 0.5 nL. After the first merging-step, the volume of the droplets increased to 43.1 ± 1.2 nL (**Figure S-3 II**). After the second merging-step, the volume of the droplets increased to 63.0 ± 1.5 nL (**Figure S-3 III**).

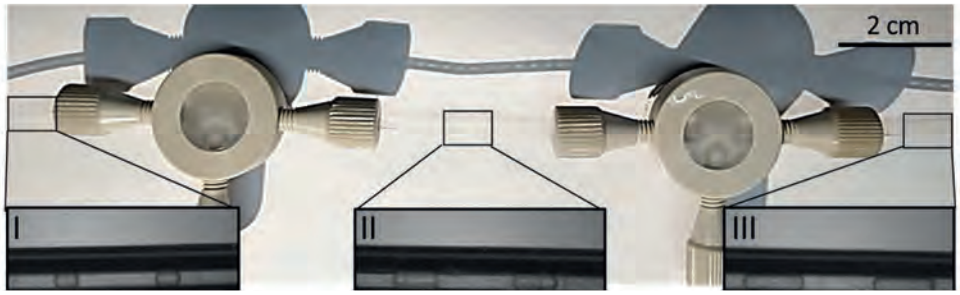

Figure S-3: droplet volumes before and after the merging steps. The shadows of the droplets are visible without magnification and give a first indication about the droplet size. For the quantification of the size, we observed the droplets at different positions of the setup with the microscope (I – III). (I) The volume of the initial droplets was determined to 23.1 ± 0.5 nL. (II) After the first merging step, the volume of droplets was determined as 43.1 ± 1.2 nL. (III) After the second merging step, the volume of droplets was determined as 63.0 ± 1.5 nL.

Reproducibility

A homogenous distribution of the magnetic beads (and other reagents) across the droplets is the basis of reproducible results. To evaluate the distribution of magnetic beads across the droplets in our system, an aqueous solution with magnetic beads, functionalized with Atto-647N-Biotin, was processed to droplets. From this train of droplets, beads were extracted at the magnetic trap in nine sequences over 10 min (**Figure S-4a**) and the fluorescence signal of the accumulated beads was detected at the magnetic trap (c(beads) = 100 µg/mL; v = 7 µL/min). The signal for each sequence increased linearly (R^2 = 0.98-0.99) with a coefficient of variance (CV) of 5 %, indicating a homogeneous distribution and reproducible extraction efficiency of the beads.

In order to analyze the inter-assay variance, three measurements of Atto-647N-Biotin dilution series were compared (**Figure S-4b**). All three measurements were performed on the same day with identical technical settings. The raw data showed a strong overlap. The slopes of the signals had an average CV of 8 %.

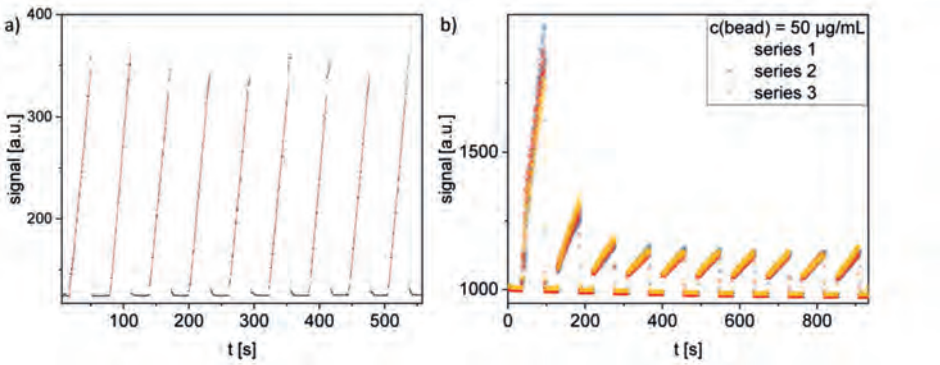

Figure S-4: Reproducibility of microfluidic measurements. (a) Distribution and extraction of the magnetic beads (CV_{slopes} = 5 %). Sequential measurements of nine identical sequences. c(beads) = 100 µg/mL, functionalized with Atto-647N-Biotin. Metal halide lamp. n = 1. (b) Inter-assay reproducibility (average CV_{slopes} = 8 %). Three independent (series 1-3) sequential measurements of ten Atto-647N-Biotin concentrations (0 - 400 pg/mL). c(beads) = 50 µg/mL. LED n = 3.

Influence of the Light Source

To enhance the sensitivity of our platform we aimed to choose an ideal light source for the Cy5-like fluorescent dyes. To that point, our system was equipped with a metal halide lamp in combination with a Cy5 excitation filter which has its emission maximum at 593 nm (**Figure S-5a**, black line). To increase the overlap with the absorption spectrum of Atto-647N-Biotin (**Figure S-5a**, red area), we replaced the metal halide lamp with an LED light source that has an emission maximum at 636 nm (**Figure S-5a**, red line), which is close to the absorption maximum of Atto-647N-Biotin at 646 nm. The LED lamp had a 2-fold higher emission intensity than the metal halide lamp at 593 nm and a 26-fold higher emission at 636 nm. Overall, the integral was 6.4 times higher for the LED in the wavelength-range of the Cy5-filter and overlapped substantially with the absorption spectrum of the fluorescent dye (**Figure S-5a**). Consequently, the LED lamp increased the slope of the linear regression by a factor of 14.4.

Furthermore, the signal/background ratio increased from the background for lower target concentrations (**Figure S-5b**). Thus, the use of the LED lamp reduced the LoD from about 100 pg/mL obtained with the metal halide lamp to appr. 8 pg/mL (**Figure S-5b**). Assuming quantitative binding of the target molecules to the beads, these concentrations equal a target-to-bead ratio at the LoD of appr. 500/1 with the metal halide lamp, and appr. 40/1 with the LED lamp. Thus, the LED lamp improves the sensitivity of our system by more than one order of magnitude.

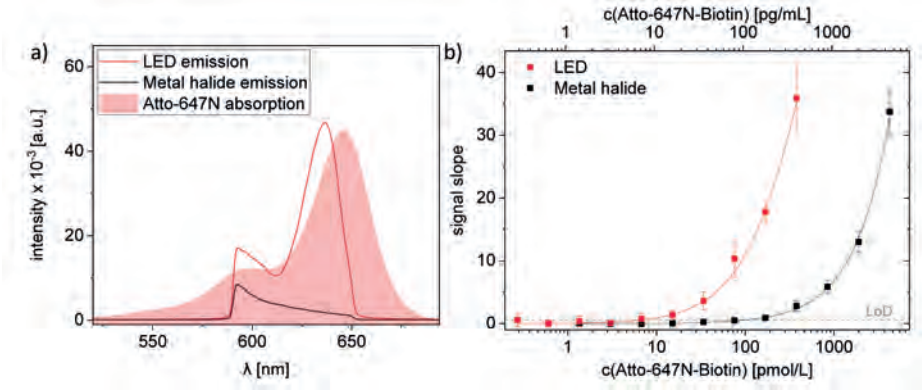

Figure S-5: Optimization of the sensitivity. (a) Emission spectra of an LED (red line) versus a metal halide (black line) light source in combination with a Cy5 excitation filter. For comparison, the absorption spectrum of Atto-647N in PBS (red, provided from www.atto-tec.com). (b) Signal slopes for Atto-647N-Biotin dilution series (0 - 400 and 0 - 4472 pg/mL) measured with a LED (red) and a metal halide (black) light source. Dashed, LoD (background + 4 x SD) of the metal halide lamp (similar for LED). Data points, mean ± SD. n = 3. Solid lines, sigmoidal fit (R^2 = 0.99). c (beads) = 100 µg/mL.

References

(1) Thedieck, K.; Holzwarth, B.; Prentzell, M. T.; Boehlke, C.; Kläsener, K.; Ruf, S.; Sonntag, A. G.; Maerz, L.; Grellscheid, S.-N.; Kremmer, E.; et al. Inhibition of MTORC1 by Astrin and Stress Granules Prevents Apoptosis in Cancer Cells. Cell 2013, 154 (4), 859–874. https://doi.org/10.1016/j.cell.2013.07.031.

(2) Origin Help - Envelope https://www.originlab.com/doc/Origin-Help/Envelope (accessed Dec 2, 2018).